Pseudorandom dynamics of frequency combs in free-running quantum cascade lasers

Citation: Henry, Nathan et al. "Pseudorandom Dynamics of Frequency Combs in Free-Running Quantum Cascade Lasers." Optical Engineering 57, 1 (September 2017): 011009 © 2017 Society of Photo-Optical Instrumentation Engineers (SPIE)

As Published: http://dx.doi.org/10.1117/1.OE.57.1.011009

Publisher: SPIE

Persistent URL: http://hdl.handle.net/1721.1/115419

Version: Final published version: final published article, as it appeared in a journal, conference proceedings, or other formally published context

Optical Engineering

OpticalEngineering.SPIEDigitalLibrary.org

Pseudorandom dynamics of frequency combs in free-running quantum cascade lasers

Nathan Henry
David Burghoff
Yang Yang
Qing Hu
Jacob B. Khurgin

SPIE.

Nathan Henry, David Burghoff, Yang Yang, Qing Hu, Jacob B. Khurgin, "Pseudorandom dynamics of frequency combs in free-running quantum cascade lasers," *Opt. Eng.* **57**(1), 011009 (2017), doi: 10.1117/1.OE.57.1.011009.

Pseudorandom dynamics of frequency combs in free-running quantum cascade lasers

Nathan Henry,[a,*] David Burghoff,[b] Yang Yang,[b] Qing Hu,[b] and Jacob B. Khurgin[a]
[a]Johns Hopkins University, Whiting School of Engineering, Baltimore, Maryland, United States
[b]Massachusetts Institute of Technology, Research Laboratory of Electronics, Department of Electrical Engineering and Computer Science, Cambridge, Massachusetts, United States

Abstract. Recent research has shown that free-running quantum cascade lasers are capable of producing frequency combs in midinfrared and THz regions of the spectrum. Unlike familiar frequency combs originating from mode-locked lasers, these do not require any additional optical elements inside the cavity and have temporal characteristics that are dramatically different from the periodic pulse train of conventional combs. Frequency combs from quantum cascade lasers are characterized by the absence of sharp pulses and strong frequency modulation, periodic with the cavity round trip time but lacking any periodicity within that period. To explicate for this seemingly perplexing behavior, we develop a model of the gain medium using optical Bloch equations that account for hole burning in spectral, spatial, and temporal domains. With this model, we confirm that the most efficient mode of operation of a free-running quantum cascade laser is indeed a pseudorandom frequency-modulated field with nearly constant intensity. We show that the optimum modulation period is commensurate with the gain recovery time of the laser medium and the optimum modulation amplitude is comparable to the gain bandwidth, behavior that has been observed in the experiments. [DOI: 10.1117/1.OE.57.1.011009]

Keywords: quantum cascade laser; frequency combs; frequency modulation.

Paper 170909SS received Jun. 13, 2017; accepted for publication Aug. 10, 2017; published online Sep. 12, 2017.

1 Introduction

Since their inception in 1994,[1] quantum cascade lasers (QCLs) have quickly become the preferred sources of coherent radiation in the mid- and far-infrared (IR) regions of the spectrum.[2] These lasers are quite versatile and can be engineered to suit specific applications, with spectroscopy being the most widespread application of QCLs due to the large number of strong fundamental absorption lines of chemical compounds in the IR and terahertz (THz) spectral ranges. THz spectroscopy is of particular interest as many large and complicated molecules, having broad and obscure absorption lines at shorter wavelengths, possess strong and narrow resonances in the THz spectral region. Due to the ease of tuning the intersubband (ISB) transition frequency, QCLs can be made to be ultrabroadband, covering spectral ranges 2 to 3 μm wide in the mid-IR and long wave-IR spectral domains.[3] Similarly, broad, almost octave spanning gain has been reported in THz QCLs.[4,5] Tunable QCL sources can be versatile, enabling components of many detection and sensing applications.[6–8] However, the tunability is usually achieved by placing the QCL gain chip inside an external cavity with a movable dispersive component (typically a grating). This fact limits the measurement speed and affects compactness and ruggedness of all spectroscopic instruments employing tunable sources, including QCLs. Tunable THz radiation is often achieved via nonlinear frequency generations that often suffer from low conversion efficiencies and output power. Another approach, using a broadband source (for example FTIR spectrometry) also requires moving components to achieve frequency selectivity.

Recent years have seen the development of an alternative approach to broadband spectroscopy involving optical frequency combs (FCs).[9] In the spectral domain, optical FCs present a series of sharp spectral lines phase locked to each other with a constant separation between two adjacent lines, i.e., the free spectral range (FSR), which is designed to closely align with the cavity resonances. When two FCs with slightly different FSRs (FSR1 and FSR2) are combined on a detector, the resulting radio frequency (RF) spectrum presents a series of sharp spectral lines (beat nodes) separated by the constant distance (FSR2-FSR1). If the intensities of one of the FCs carry information on the transmission (absorption) through the medium of spectroscopic interest, at the detector this information is instantly transferred into the RF domain. Thus, fast detection is accomplished without any moving components and using only a single detector rather than an array of detectors.

Once the advantages of this "dual-comb spectroscopy" method were fully comprehended, a strong effort was mounted to develop robust FC sources from UV to far-IR. While there have been successes in generating FCs using CW-pumped microresonators,[10] the best octave-spanning FC sources all incorporate mode-locked lasers generating infinite trains of ultrashort pulses, whose Fourier transform constitutes FCs. The best examples of mode-locked lasers are Ti-sapphire lasers producing combs close to the visible range and various fiber lasers whose wavelengths lie in near-IR below 2.5 μm.[11,12] When it comes to extending the range

*Address all correspondence to: Nathan Henry, E-mail: nhenry7@jhu.edu

of FCs into the mid- and far-IR spectral regions, one is forced to rely on nonlinear frequency conversion techniques (difference frequency generation or optical parametric amplification).[13] This greatly increases the complexity of the FC generating apparatus and reduces its efficiency. It would be far more preferable to obtain FC directly from a mid- to far-IR source, such as the QCL.

Alas, passive mode-locking has not been achieved in QCLs because the ISB transitions have inherently short relaxation (gain recovery) times, on the order of $\tau_2 \sim 1$ ps when compared to the cavity round trip times that are on the order of $\tau_{rt} \sim 100$ ps.[14] Mode-locking typically requires a gain medium with gain recovery times that are much longer than τ_{rt} such that the energy can be effectively stored in the upper laser level (ULL) in between pulses. Indeed in an all solid state or fiber laser amenable to mode-locking, the gain recovery time is measured in at least hundreds of microseconds while the cavity round trip times are no longer than tens of nanoseconds.

Active mode-locking of QCL's in external cavities have been reported;[15–17] however, both the period and pulse length achieved were very long and with a very large duty cycle resulting in a spectrum consisting of very few, broad spectral lines, making spectroscopic applications unworkable. It is well known that active mode-locking can never reach the bandwidth that could be provided by a passive mode-locking regime of operation. However, in addition to the aforementioned long gain recovery time, passive mode-locking requires incorporation of a saturable absorber with a very short recovery time inside the cavity. Fast saturable absorbers present lower loss to a train of sharp pulses than to that of CW radiation. This causes the formation of mode-locked pulses to arise from noise, as pulses get sharpened with each successive pass through the absorber until their spectral bandwidth approaches the width of the gain. QCL gain media, due to an inherently short gain recovery time, presents fast saturable gain (rather than loss), which is exactly the opposite of what is needed for mode-locking. Therefore, any pulse in the QCL gain media is expected to flatten with each successive pass until a constant intensity oscillation is achieved.

However, notwithstanding this admittedly pessimistic outlook for FC generation in QCLs, the stable FC operation of QCL in the mid-IR has been reported by the ETH Zurich group[18] and later confirmed by numerous other groups[19,20] including FC generation in THz QCLs.[4] Furthermore, the stability, narrow linewidth, and equal spacing of QCL FCs[21] have been good enough to enable their application in dual-comb spectroscopy in both mid-IR[22] and THz[23] spectral domains. Experimental evidence has shown that FCs are indeed generated by free-running QCL lasers[4,18] as long as the gain medium is sufficiently broadband and, most critically, provided that a good dispersion compensation is achieved. The salient feature of all QCL FCs is that the time domain intensity looks like anything but the short pulses generated by the conventional mode-locked laser. Instead, the intensity varies around some constant value while the instant frequency varies periodically with the round trip time.

The key to understanding the genesis of FCs in a gain media with short τ_2 lies in realizing that stable FCs only require some stable phase relation between the frequency lines (longitudinal modes) and that conventional mode-locking, in which all the phases are equal, is only one of an infinite number of phase relations. Some of these combinations result in constant intensity radiation with periodically modulated instant frequency, commonly known as frequency-modulated (FM) lasing.[24] Now, since the broad gain in a QCL is usually achieved by variations of the thickness of quantum wells in different periods of QCL-active layers, a certain amount of inhomogeneous broadening will cause spectral hole burning to always be present. In addition, spatial hole burning is bound to occur in a Fabry–Pérot cavity. This hole burning in spectral and spatial domains favors multimode operation. Indeed, any Fabry–Pérot QCL usually operates in the multimode regime and single mode operation is only attainable in the DFB QCL.[25] At the same time, a short gain recovery time in the QCL favors constant intensity operation. The only way in which nearly constant intensity can coexist with multimode operation is the FM regime that has indeed been observed in Refs. 4 and 18.

2 Frequency-Domain Model of Self-FM Operation

This phenomenological rationalization of self-FM operation of free-running QCLs has been confirmed by a theoretical model that was developed in Ref. 26 via a perturbative solution of the set of Maxwell Bloch equations in the frequency domain (i.e., solving a separate Maxwell equation for each mode). In this model, the phase relations among the different modes arise from the four-wave mixing (FWM) between them. The FWM in QCLs is engendered by the rapid oscillations of the gain at the intermode beat frequency, i.e., it is a real rather than virtual FWM process that is responsible for FC formation in dielectric resonators.

Rather unexpectedly, the model also predicted what we shall call a "pseudorandom" FM signal in a sense that it is periodic with the round trip time τ_{rt}, yet strongly irregular on shorter time scales, as shown in Fig. 1(a). This figure shows the oscillations of the instant frequency $\nu(t)$ of the FM signal $E(t) = E_0 \exp[2\pi i \int \nu_R(t) dt]$, where $|\nu_R(t)| \leq A_{FM}$ and is normalized to τ_{rt}^{-1} around the central (carrier) frequency ν_0. As one can see, within each period the instant frequency oscillates around some mean value aperiodically but with a mean oscillation period $\langle T_{FM} \rangle$ that is commensurate with the gain recovery time τ_2 and the amplitude of FM A_{FM} commensurate with the half-bandwidth of the gain.

At the time of writing,[26] the explanation of "pseudorandomness" was not given, and it was even thought that the aperiodicity can simply be traced to the fact that the phase relation among the modes arises initially from some random noise; hence, it would be possible to obtain a more deterministic fully periodic FM signal, especially if one can "seed" it by modulating the current. However, multiple experimental data accumulated in the last couple of years indicate that far from being a fluke, the "pseudorandom" FM is indeed a preferred operating regime of a free-running QCL with a well-compensated dispersion. What we mean as the "preferred" operating regime is the regime that has the lowest threshold, i.e., the regime in which the photons, on average, experiences the highest net gain as they pass through the active region. It is the goal of this work to explicate the pseudorandomness of the self-FM regime in QCL FCs, in the hope that eventually it may allow us to exert some control over FC characteristics.

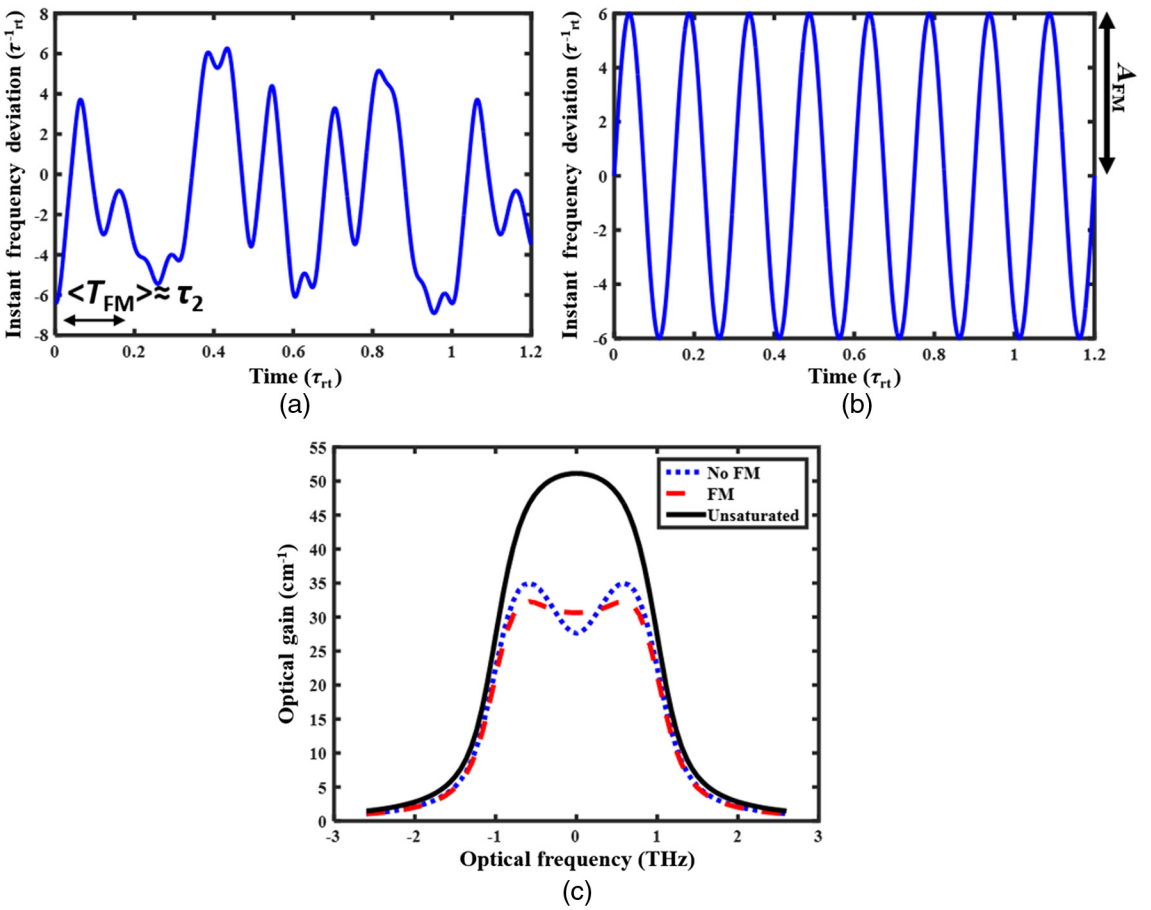

Fig. 1 (a) Pseudorandom frequency modulation simulated in Ref. 26. (b) Deterministic, single frequency modulation. (c) Gain profile after lasing with and without frequency modulation. Intracavity power is 25 mW or 30% of the averaged saturation power, $\bar{P}_{sat}$.

First, let us present some qualitative arguments for pseudorandomness of self-FM in the QCL. Consider an inhomogeneously broadened (spectral inhomogeneity has not been taken into account in Ref. 26) gain profile shown Fig. 1(c), typical for a broadband THz QCL[4] and similar to the gain in mid-IR QCLs. When lasing occurs at a single mode, the gain saturates strongly in the middle (a spectral hole is burned) and the effective gain experienced by the signal is reduced. When the frequency is modulated, the spectral hole burning is mitigated and the effective gain increases. Hole burning mitigation occurs when the instant frequency moves away from the saturated spectral region and comes back when the gain has been replenished, i.e., at a time comparable to the gain recovery time τ_2. If the instant frequency does not sweep the whole gain spectrum within the gain recovery time, a significant fraction of the pump energy stored on the ULL will be lost to nonradiative ISB relaxation. Clearly, this disqualifies the simplest FM signal $\nu(t) = A_{FM}\ \sin(2\pi t/\tau_{rt})$ with a period $\tau_{rt} \gg \tau_2$. Since the FM signal is repeated every round trip time, it appears that a suitable form of it would be a "nice" FM signal shown in Fig. 1(b) with instant frequency varying as

$$\nu_R(t) = A_{FM}\ \sin(2\pi m t/\tau_{rt}), \tag{1}$$

where m is an integer number on the scale of $m \sim \tau_{rt}/\tau_2$ which can be as large as 50. However, while this signal looks perfectly acceptable from the point of view of spectral hole mitigation, it badly fails to address spatial hole burning because its spectrum contains spectral lines separated by m/τ_{rt}, indicating that only one out of each m modes would be lasing. This would greatly exacerbate spatial hole burning and is rarely seen in experiment at narrow bias ranges. When the FM is pseudorandom within τ_{rt}, as shown in Fig. 1(a),

$$\nu_R(t) = A_{FM}\ \sin[2\pi\nu_{FM}(t)t] \tag{2}$$

yet periodic with the round trip frequency, i.e., $\nu_{FM}(t+\tau_{rt}) = \nu_{FM}(t)$, each mode within the gain bandwidth is active, which mitigates spatial hole burning. With a modulation signal that is pseudorandom yet periodic with a mean period commensurate with τ_2, the gain can be efficiently and uniformly saturated while maintaining an FC spaced by the round trip frequency.

To confirm this rather simple qualitative explanation, we developed a rigorous time-domain model that goes beyond the one used in Ref. 26, which did not take into account spectral hole burning, was perturbative in nature (only third-order terms were included), and did not take into account the coherent effects occurring at the time scale commensurate with the coherence time τ_{coh}. The model developed below addresses all the shortcomings of the prior work and convincingly shows that the pseudorandom self-FM operating

mode is indeed a natural operating regime of QCL resulting in stable FC generation.

Given the large number of parameters involved in QCL modeling and the fact that many of these parameters, such as lifetimes, tunneling times, transition dipole matrix elements etc., cannot be independently determined with perfect precision, one cannot expect our model to accurately predict all operating characteristics of any actual THz QCL laser and, therefore, be used as a design tool. The purpose of this work is less ambitious yet, in our view, more stimulating—to establish that a typical THz QCL with dispersion compensation is expected to operate in a pseudorandom FM regime. In this work, we use parameters in line with the device reported in Ref. 4, but our conclusions are valid for the wide range of THz QCL characteristics as long as they satisfy the requirements of short gain recovery time, broad gain, and compensated dispersion.

3 Time-Domain Model of Inhomogeneously Broadened QCL

We can describe the effects of FM by approximating the gain dynamics with the optical Bloch equations (OBEs) for an inhomogeneously broadened system. First, as shown Fig. 2(a), we approximate each period of the QCL-active region by an effective three-level scheme comprised of the injection level (level 3), ULL 2, and lower laser level 1 (LLL), subsequently followed by the next injection level. As shown in Fig. 2, the lifetime of the ULL is τ_2, depopulation of the LLL is achieved at a rate τ_1^{-1} and injection into the ULL from level 3 occurs at a tunneling rate τ_t^{-1}. While a single period of the QCL is in fact comprised of more than three levels, it is desirable to reduce the model to a two-level system in order to decrease computational requirements. In a typical THz QCL, this approximation is close to the reality (typical a THz QCL period has four to five levels) while in a mid-IR QCL there are more injector layers between levels 1 and 3. It is fairly obvious, however, that the depopulation time τ_1 in our simplified model is the effective time that includes the relaxation rate of LLL per se and the transport through the injector to the level 3.

The model's equations are derived via OBEs, with the usual rotating wave and slow envelope approximations. The inhomogeneously broadened three-level system is described by a set of N density matrices $\rho^{(n)}$, with lasing transitions having resonance frequencies $\omega_{21}^{(n)}$ spread around the mean transition frequency $\bar{\omega}_{21}$ according to a normalized distribution function $f^{(n)} = f(\omega_{21}^{(n)} - \omega_{21})$, the shape of which can be surmised from Fig. 1(c). Due to charge neutrality, the

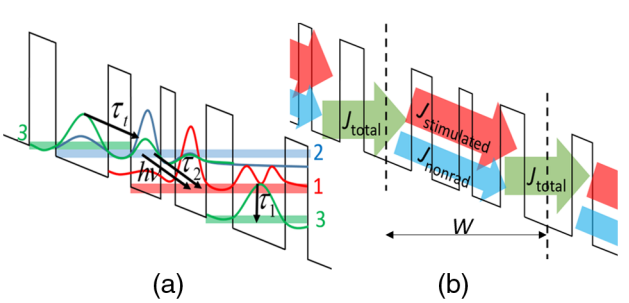

Fig. 2 (a) Drawing of levels in one period of QCL and (b) dissection of current, recycled through periodic structure.

populations of the three levels are related to the diagonal density matrix elements as $N_i = N_{2\text{-D}} \sum_n^N f^{(n)} \rho_{ii}^{(n)}$ where $N_{2\text{-D}}$ is the two-dimensional (2-D) doping density and $\sum_{i=1.}^{3} \rho_{ii}^{(n)} = 1$ which allows us to not consider $\rho_{33}^{(n)}$ in the rate equations. For each spectral bin, the 2×2 density matrix $\rho^{(n)}$ evolves as

$$\frac{d}{dt}\rho^{(n)} = -\frac{j}{\hbar}[H_0^{(n)} + H_{\text{filed}}^{(n)}, \rho^{(n)}] + R^{(n)}, \tag{3}$$

where

$$H_0^{(n)} = \hbar \begin{bmatrix} \omega_{21}^{(n)}/2 & 0 \\ 0 & -\omega_{21}^{(n)}/2 \end{bmatrix} \tag{4}$$

and interaction with the optical field Hamiltonian is

$$H_{\text{field}} = \hbar \begin{bmatrix} 0 & \Omega \cos[\omega_0 t + \phi_{\text{FM}}(t)] \\ -\Omega \cos[\omega_0 t + \phi_{\text{FM}}(t)] & 0 \end{bmatrix}. \tag{5}$$

Here $\Omega = qz_{12}E_0/\hbar$ is the Rabi frequency and $z_{12} = \int \Psi_1^* z \Psi_2 dz$ is the dipole moment of the transition.

The phenomenologically introduced pumping/scattering matrix is then

$$R^{(n)} = \begin{bmatrix} \rho_{22}^{(n)}\tau_2^{-1} - \rho_{11}\tau_1^{-1} & -\rho_{11}^{(n)}\tau_{\text{coh}}^{-1} \\ -\rho_{21}^{(n)}\tau_{\text{coh}}^{-1} & J^{(n)}/qf^{(n)}N_{2\text{-D}} - \rho_{22}^{(n)}\tau_2^{-1} \end{bmatrix}, \tag{6}$$

where τ_{coh} is the coherence time and $J^{(n)} = f^{(n)}J$ is the fraction of the total current density J, carried by the fraction of 2-D electrons passing through the QW's with resonant frequency $\omega_{21}^{(n)}$. Obviously, this means that in the absence of lasing, the density matrix for each spectral bin is pumped to the same initial state $\rho_{22,0}^{(n)} = J\tau_2/qN_D$; $\rho_{11,0}^{(n)} = \rho_{22,0}^{(n)}\tau_1/\tau_2$ with the population inversion $\Delta\rho_0^{(n)} = J(\tau_2 - \tau_1)/qN_D$. As the QCL is pumped by a constant current source, we can write for the total current density

$$\frac{J}{qN_{2\text{-D}}} = \frac{\rho_{33}^{(n)} - \rho_{22}^{(n)}}{\tau_t^{(n)}} = \frac{\rho_{11}^{(n)}}{\tau_1^{(n)}}. \tag{7}$$

This means that once lasing commences both the tunneling time and the effective depopulation time will change to assure that the current remains constant (but the voltage drop on each QCL period will change). Because $\sum_{i=1.}^{3} \rho_{ii}^{(n)} = 1$, one obtains $J = qN_D/(\tau_1 + 2\tau_2 + \tau_t)$ and the maximum population inversion attainable in the QCL is $\Delta\rho_{\max}^{(n)} = (\tau_2 - \tau_1)/(\tau_1 + 2\tau_2 + \tau_t) < 1/2$. With doping densities in the $\sim 1 \times 10^{10}$ cm^{-2} range and depopulation values in the few ps range, one can expect current densities on the order of 500 A/cm^2.

With all of the above definitions Eq. (3) becomes

$$\frac{d}{dt}\rho_{11}^{(n)} = j(\rho_{21}^{(n)}\Omega - \rho_{12}^{(n)}\Omega)\cos[\omega_o t + \phi_{\mathrm{FM}}(t)] + \frac{\rho_{22}^{(n)}}{\tau_2} - \frac{\rho_{11}^{(n)}}{\tau_1},$$
$$\frac{d}{dt}\rho_{22}^{(n)} = -j(\rho_{21}^{(n)}\Omega - \rho_{12}^{(n)}\Omega)\cos[\omega_o t + \phi_{\mathrm{FM}}(t)] + \frac{J}{qN_d} - \frac{\rho_{22}^{(n)}}{\tau_2}$$
$$\frac{d}{dt}\rho_{21}^{(n)} = -j\omega_{21}^{(n)}\rho_{21}^{(n)} - j(\rho_{22}^{(n)} - \rho_{11}^{(n)})\Omega\cos[\omega_o t + \phi_{\mathrm{FM}}(t)] - \frac{\rho_{21}^{(n)}}{\tau_{\mathrm{coh}}}. \tag{8}$$

Introducing the rotating wave approximation $\rho_{21} = \sigma_{21}e^{-j\omega_o t - \phi_{\mathrm{FM}}(t)}$ and $\rho_{12} = \sigma_{12}e^{+j\omega_o t + \phi_{\mathrm{FM}}(t)}$, we obtain from Eq. (8)

$$\frac{d}{dt}\rho_{11}^{(n)} = -\Omega\,\mathrm{Im}(\sigma_{21}^{(n)}) + \frac{\rho_{22}^{(n)}}{\tau_2} - \frac{\rho_{11}^{(n)}}{\tau_1},$$
$$\frac{d}{dt}\rho_{22}^{(n)} = \Omega\,\mathrm{Im}(\sigma_{21}^{(n)}) + \frac{J}{qN_d} - \frac{\rho_{22}^{(n)}}{\tau_2},$$
$$\frac{d}{dt}\sigma_{21}^{(n)} = -j\sigma_{21}^{(n)}(\omega_{21}^{(n)} - \omega_o - \omega_{\mathrm{FM}}) - j(\rho_{22}^{(n)} - \rho_{11}^{(n)})\frac{\Omega}{2} - \frac{\sigma_{21}^{(n)}}{\tau_{\mathrm{coh}}}. \tag{9}$$

Now, expressing the level populations as $\rho_{11}^{(n)} = J\tau_1/qN_{2\text{-D}}$ and $\rho_{22}^{(n)} = \Delta\rho + J\tau_1/qN_{2\text{-D}}$, we immediately get a result for the population inversion $\Delta\rho^{(n)}$ and polarization $\sigma_{21}^{(n)}$ of the n'th inhomogeneously broadened transition

$$\frac{d}{dt}\Delta\rho^{(n)} = 2\frac{J}{qN_d}\left(1 - \frac{\tau_1}{\tau_2}\right) - \frac{2\Delta\rho^{(n)}}{\tau_2} + 2\Omega\,\mathrm{Im}(\sigma_{21}^{(n)}),$$
$$\frac{d}{dt}\sigma_{21}^{(n)} = -j[\omega_{21} - \omega_n + \omega_{\mathrm{FM}}(t)]\sigma_{21}^{(n)} - j\Delta\rho^{(n)}\frac{\Omega}{2} - \frac{\sigma_{21}^{(n)}}{\tau_{\mathrm{coh}}}. \tag{10}$$

Finally, after we normalize the time and all relevant frequencies to the coherence time as

$$\tau = t/\tau_{\mathrm{coh}},$$
$$\Omega' = \Omega\tau_{\mathrm{coh}},$$
$$\Delta\omega_n'(t) = [\omega_{21}^{(n)} - \omega_o + \omega_{\mathrm{FM}}(t)]\tau_{\mathrm{coh}}, \tag{11}$$

we obtain what amounts to be OBEs (splitting the polarizations, σ_{21}, into real and imaginary parts)

$$\frac{d}{d\tau}\Delta\rho^{(n)} = \frac{2(\Delta\rho_o - \Delta\rho^{(n)})}{T} + 2\Omega'\,\mathrm{Im}(\sigma_{21}^{(n)}),$$
$$\frac{d}{d\tau}\sigma_{21}^{(n)} = -j\Delta\omega_n'(\tau)\sigma_{21}^{(n)} - j\Delta\rho^{(n)}\frac{\Omega'}{2} - \sigma_{21}^{(n)}, \tag{12}$$

where $T = \tau_2/\tau_{\mathrm{coh}}$. We shall refer to Eq. (12) as the "coherent" equations as it takes into account dynamics of the polarization on a scale comparable to or faster than τ_{coh}. If, on the other hand, the rate of FM is slower than coherence time, i.e., $d/d\tau \ll 1$, then the polarization follows the optical field adiabatically as:

$$\sigma_{21}^{(n)}(t) = -\frac{1}{2}j\Delta\rho^{(n)}\Omega'/[1 + j\Delta\omega_n'(t)], \tag{13}$$

and one obtains the "incoherent" or "rate equation" approximation from the dynamics of level populations only.

$$\frac{d}{d\tau}\Delta\rho^{(n)} = \frac{2(\Delta\rho_o - \Delta\rho^{(n)})}{T} - \frac{\Omega'^2\Delta\rho^{(n)}}{1 + \Delta\omega_n'^2(\tau)}. \tag{14}$$

Now, before we proceed, it makes sense to introduce the relation between the variables in the rate equation and actual observable parameters of the QCL. We define the instant saturation intensity for each "frequency bin" as

$$I_{\mathrm{sat}}^{(n)}(\tau) = \frac{\bar{n}\hbar[1 + \Delta\omega_n'^2(\tau)]}{\tau_2\tau_{\mathrm{coh}}z_{21}^2 4\pi\alpha_o}, \tag{15}$$

where α_0 is the fine structure constant and $\bar{n}$ is the background index, and rewrite (14) as

$$\frac{d}{d\tau}\Delta\rho^{(n)} = \frac{2\Delta\rho_o}{T} - \frac{2\Delta\rho^{(n)}}{T}[1 + I/I_{\mathrm{sat}}^{(n)}(\tau)]. \tag{16}$$

The mean saturation intensity at which the gain decreases to half its original value can be found out as

$$\bar{I}_{\mathrm{sat}} = \frac{\bar{n}\hbar(1 + \Delta\bar{\omega}'^2)}{\tau_2\tau_{\mathrm{coh}}z_{21}^2 4\pi\alpha_o}, \tag{17}$$

where the value of $\Delta\bar{\omega}'$ is commensurate with $\Delta\omega_{\mathrm{gain}}\tau_{\mathrm{coh}}$, i.e., the ratio of inhomogeneous and homogeneous broadening. Using typical values as mentioned earlier and estimating a dipole moment, z_{21} of 3 to 6 nm for THz we arrive with a saturation intensity in the vicinity of 500 MW/cm^2. It is important that the laser achieve some level of intensity that is not too much less than $\bar{I}_{\mathrm{sat}}$ as the effects gained by FM will not be prevalent otherwise.

We shall also establish a relation between the density matrix elements in Eqs. (12) and (14) and another observable parameter, gain. For that we first find the expected value of the dipole moment for each transition n,

$$\langle\mu^{(n)}\rangle = Tr(\rho^{(n)}\mu) = qTr\left[\begin{pmatrix}\rho_{11}^{(n)} & \rho_{12}^{(n)}\\ \rho_{21}^{(n)} & \rho_{22}^{(n)}\end{pmatrix}\begin{pmatrix}0 & z_{12}\\ z_{21} & 0\end{pmatrix}\right]$$
$$= qz_{21}\sigma_{21}^{(n)}e^{j\omega t} + c.c. \tag{18}$$

The material polarization is then

$$P(t) = \frac{N_{2\text{-D}}}{W}\sum_N\langle f_n\mu^{(n)}\rangle$$
$$= \frac{2N_{2\text{-D}}}{W}\frac{q^2z_{21}^2\tau_{\mathrm{coh}}}{\hbar\Omega'}\sum_N f_n\sigma_{21}^{(n)}(t)\frac{E_0}{2}e^{j\omega t} + c.c., \tag{19}$$

where W is the period thickness. Substituting Eq. (19) into the Helmholtz equation for the slow variable envelope

$$2jk_0\bar{n}\frac{dE}{dz} = -\frac{\omega_0^2}{c^2\epsilon_o}P, \tag{20}$$

we obtain

$$\frac{dE_0}{dz} = k_0 \frac{N_{2\text{-D}}}{W} \frac{q^2 z_{21}^2 \tau_{\text{coh}}}{\bar{n}\epsilon_o \hbar \Omega'} \sum_N f_n \, \text{Im}\sigma_{21}^{(n)}(t) E_0 = \frac{\gamma}{2} E_0. \quad (21)$$

Hence, the instant gain coefficient is

$$\gamma(t) = \Gamma \frac{8\pi\alpha_0 N_{2\text{-D}} z_{21}^2}{n_{\text{eff}} W} \omega \tau_{\text{coh}} \sum_N f_n \frac{\text{Im}\sigma_{21}^{(n)}(t)}{\Omega'(t)}, \quad (22)$$

where the Rabi frequency is in general time-dependent (to accommodate amplitude-modulated signals), and we introduced the confinement factor of the cavity Γ and the effective mode index n_{eff}. In THz QCLs $\Gamma \sim 1$ due to the confinement of the metal–metal waveguide, and $n_{\text{eff}} \approx \bar{n}$. For mid-IR lasers, the confinement factor is somewhat smaller, but the effective index is not changed much.

With the incoherent approximation Eq. (13), the instant gain reduces to

$$\gamma(t) = \Gamma \sum_n f^{(n)} \frac{4\pi\alpha_0}{n_{\text{eff}}} \frac{N_{2\text{-D}}}{W} \frac{z_{21}^2 \omega_o \tau_{\text{coh}} \Delta\rho^{(n)}}{(1 + \Delta\bar{\omega}'^2)}. \quad (23)$$

Now, in order to find out which FM format leads to the lowest threshold of the QCL in the presence of spatial hole burning, we will eventually need to solve the equations for density matrix elements Eqs. (12) or (14) in which the variables depend not only on time and frequency but also on the spatial coordinate z, where the step of z should be much less than wavelength. This may present computational difficulties, therefore, prior to going full throttle and incorporating spatial hole burning, we shall investigate whether the full coherent model is necessary by considering only spectral hole burning.

4 Time-Domain Model with Spectral Hole Burning

Now we shall attempt to answer the following question: given the gain profile of Fig. 1(c) that is both homogeneously (FWHM $= \tau_{\text{coh}}^{-1}$) and inhomogeneously (FWHM $= \Delta\omega_{\text{gain}}$) broadened, and possessing a short gain recovery time τ_2, what type of operating regime will have the lowest possible threshold? As shown in Fig. 2(b), in each active region the injected current follows two parallel paths: either via nonradiative transitions to the LLL (relaxation current) or via the stimulated emission. Since it is stimulated transitions that account for the laser gain while the nonradiative decay amounts to waste, the regime in which photons experience the highest gain will be the one that possesses the lowest threshold and will actually oscillate. The process that forces the radiation arising from noise to conform to the most efficient regime is FWM and cross-phase modulation inside the gain medium, and to model it exactly in time domain would be very time consuming. However, in our prior work, in the frequency domain,[26] we have shown how this is indeed the case, and FWM causes the laser to operate in the most efficient regime. Thus, in this study, we are interested only in determining what the parameters of this efficient regime are.

We, therefore, consider periodic FM signals, with instant frequency varying as $\nu_R(t) = A_{\text{FM}} \sin(2\pi t/T_{\text{FM}})$ and monitor two parameters: average gain experienced by photons $\bar{\gamma} = T_{\text{FM}}^{-1} \int_t^{t+T_{\text{FM}}} \gamma(t) \text{d}t$ and the average relaxation current $\bar{J}_{\text{rel}} = q\tau_2^{-1} T_{\text{FM}}^{-1} \sum_n f_n \int_t^{t+T_{\text{FM}}} \Delta\rho^{(n)}(t) \text{d}t$.

The device parameters used in our simulation have been chosen to correspond to a "diagonal transition" THz QCL that has successfully produced FCs,[4,27,28] having a broad gain with $\Delta\nu_{\text{gain}} = 2$ THz centered at the lasing frequency of $\nu_0 = 3$ THz, a dipole moment $z_{12} = 5$ nm, gain recovery time $\tau_2 = 4$ ps, coherence time $\tau_{\text{coh}} = 0.7$ ps, and LL depopulation time $\tau_1 = 0.5$ ps. The active region of the QCL is doped with 2-D doping density $N_{2\text{-D}} = 3.5 \times 10^{10}$ cm^{-2} over an effective thickness of one period, $W = 57$ nm.

Injected current density is $J = 500$ A/cm^2, and the power inside the cavity is ~25 mW corresponding to $\Omega' = 0.78$. With these values, we can calculate a saturation power of ~83 mW given an absolute value of average detuning $\Delta\bar{f} = 0.5$ THz, hence the intracavity power of 25 mW amounted to 30% of the saturation intensity and an unsaturated gain around 50 cm^{-1}. This is sufficient to exceed the laser threshold by a factor approaching 1.5 to 2 and cause saturation that should make the differences between various FM regimes tested below discernible. All of these values are in general agreement with experimental results.[4,27–29]

The results of modeling using both coherent (OBE) and incoherent (rate equations) approaches are shown in Fig. 3. In Fig. 3(a), the value of the average gain $\bar{\gamma}$ versus T_{FM} is shown for the two approaches and compared to the no-FM case (circles). Clearly, FM does increase the effective gain experienced by the photons and reduces the wasteful relaxation current. Both "coherent" and "incoherent" approaches show the same trend for large FM periods—a steady decline as T_{FM} increases. This is a predictable trend, for a large T_{FM}, the instant frequency of the laser would dwell in the same spectral region for a time longer than τ_2; hence, the spectral hole would have enough time to develop and $\bar{\gamma}$ would decrease. At the same time, population inversion outside the spectral hole region remains undepleted by stimulated emission, which causes an increased relaxation current $\bar{J}_{\text{rel}}$ as can be seen from the curves in Fig. 3(b) [which, as expected, are complimentary to the curves in Fig. 3(a)].

However, at short FM periods, the "coherent" and "incoherent" gain curves diverge with incoherent gain exhibiting a continuing increase while the coherent gain takes a sharp dive. This decline is entirely predictable as when the period of modulation becomes first commensurate and then shorter than the coherence time the two-level system no longer responds to FM modulation, and hence, all the benefits of sweeping the instant frequency over the gain bandwidth get lost. In other words, the coherent model predicts that there exists the optimum frequency of FM modulation, commensurate with $\tau_2 > \tau_{\text{coh}}$ such that on one hand, the frequency sweeps through the entire gain bandwidth at a rate slightly faster than the gain recovery time and on the other hand, the sweep is sufficiently slow for the system to respond to it.

Once the FM period exceeds roughly $\tau_2/2$, both "coherent" and "incoherent" models behave similarly showing nearly identical slopes of the $\bar{\gamma}$ versus T_{FM} curves, hence, if one restrains T_{FM} to the values commensurate with τ_2 one can use the rate equation model to determine the most efficient QCL operating regime with a high degree of confidence. We shall use this fact in our work in the following sections.

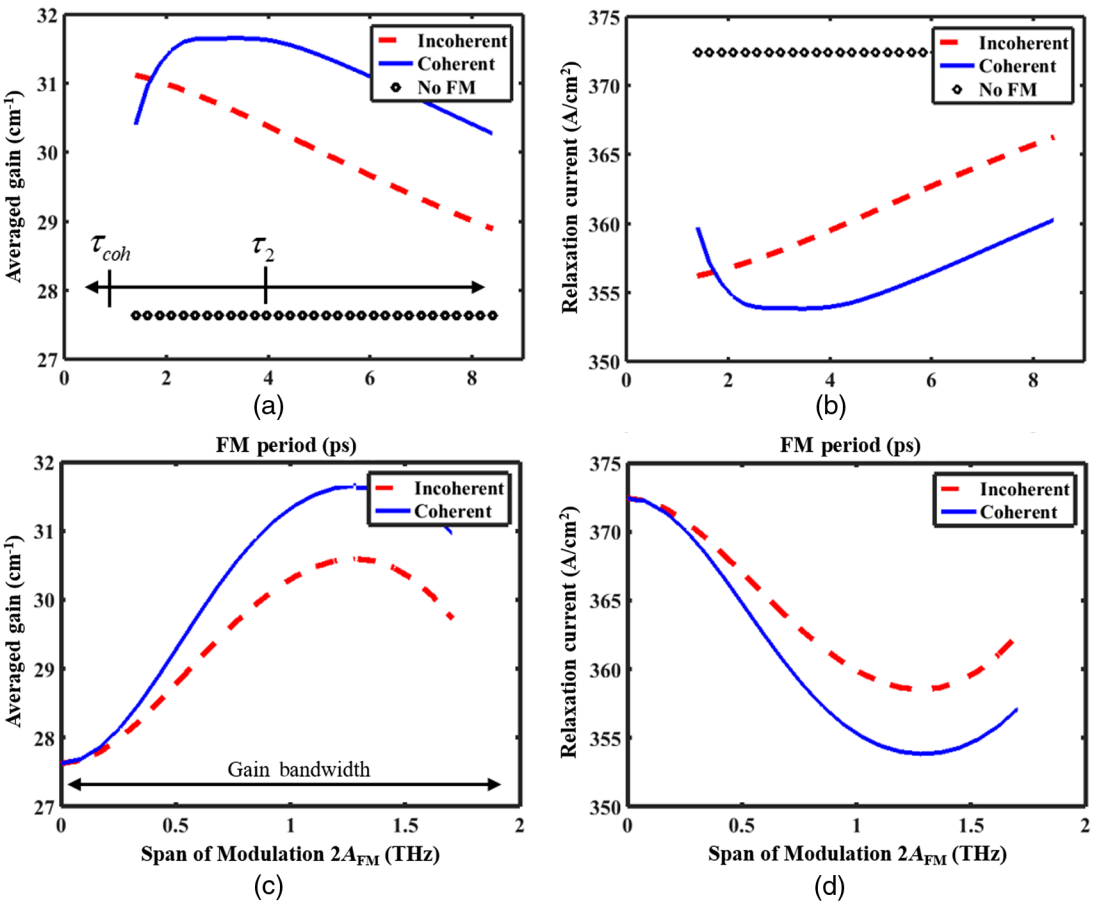

Fig. 3 Averaged gain and relaxation current versus (a, b) FM signal period and (c, d) modulation amplitude. The data presented here are generated using a purely sinusoidal FM signal without any pseudorandom nature. The span of modulation used for (a, b) is 1.2 THz, the optimum as shown in (c, d). The period of modulation in (c, d) is 2.88 ps, the optimum shown in (a, b).

The results plotted in Figs. 3(a) and 3(b) have been obtained for the FM span $2A_{FM} = 1.2$ THz, which is optimum as follows from the curves in Figs. 3(c) and 3(d). The period for Figs. 3(c) and 3(d) is 2.88 ps, which is the optimum value as shown in Figs. 3(a) and 3(b). Figures 3(c) and 3(d) show the relation between gain and relaxation current with the span of the FM signal, in this case the span is twice that of A_{FM} in order for a direct comparison to be made with the gain bandwidth. This result is obviously intuitive since the FM amplitude should be sufficient enough to sweep the entire gain bandwidth effectively but should not be any larger. Note that both coherent and incoherent approaches yield the same value of optimum FM amplitude and also that the curves in Figs. 3(c) and 3(d) are complimentary, as expected.

At this point, the model is generally ambivalent in regards to whether the modulating signal is a single frequency or a pseudorandom signal. It is not until the introduction of spatial hole burning that the pseudorandom nature of the modulation signal comes into play.

5 Impact of Amplitude Modulation

Before introducing spatial hole burning into our model, it is a useful exercise to explore the effect of introducing amplitude modulation in addition to frequency modulation. This is very likely to occur in QCL devices as a result of cavity dispersion, and in fact, simultaneous AM and FM is always seen in real devices.[30] In addition to this, one can expect some level of AM to arise from the process of frequency modulation itself. As the mode is FM and approaches the edge of the gain, one would expect a decrease in the gain seen and thus some modulation of intensity. As expected, the effect of AM is exactly opposite that of FM, namely the gain experienced by the light decreases with increasing AM depth. As we have mentioned already, the medium with the fast saturable gain always favors the CW amplitude and ideally (meaning no dispersion and a very broad spectrum) will keep "flattening" the signal until CW amplitude is achieved as shown in our frequency domain model.[26]

This clearly highlights the necessity to avoid FM-to-AM conversion by designing proper dispersion compensation techniques. It is also important to note that while AM will always be present, it is usually not so strong as to turn the radiation off completely let alone to form short pulses.

6 Introducing Spatial Hole Burning

We now turn our attention to the main issue facing us, namely how does spatial hole burning select the most effective operating regime of the QCL? Obviously, if the laser operates in a single longitudinal mode, the intensity inside the cavity will have a pattern of peaks and troughs, and

the spatial holes will be burned wherever the peaks are. At this point, the model is developed to be three-dimensional (3-D) in that it tracks the population for position, time, and spectral frequency.

Let us examine what will happen if the frequency is modulated in a deterministic fashion with a constant FM period, T_{FM}, as discussed above. The forward propagating FM field as a function of position z inside the cavity can be written as

$$E(z,t) = \frac{1}{2}E_0 \exp\left\{-j2\pi\nu_0\left(t - z\frac{n_{\mathrm{eff}}}{c}\right) - j\frac{A_{\mathrm{FM}}}{\nu_{\mathrm{FM}}}\cos\left[2\pi\nu_{\mathrm{FM}}\left(t - z\frac{n_{\mathrm{eff}}}{c}\right)\right]\right\} + c.c, \quad (24)$$

where $A_{\mathrm{FM}}/\nu_{\mathrm{FM}} = A_{\mathrm{FM}}T_{\mathrm{FM}} = A_{\mathrm{FM}}\tau_{\mathrm{rt}}/m$ is the frequency modulation index. When two counterpropagating waves delayed by the delay time $\Delta t = 2zn_{\mathrm{eff}}/c$ interfere inside the cavity the resulting intensity averaged over $T_{\mathrm{FM}} \sim \tau_2$ becomes

$$\langle E^2(z)\rangle = \frac{E_0^2}{2}\left[1 + J_0\left(\frac{A}{2\pi\nu_{\mathrm{FM}}}\sin m\pi z/L\right)\cos(8\pi z/\lambda)\right] \quad (25)$$

as shown in Fig. 4(a). Now, one can see that when two counterpropagating FM waves interfere inside the cavity they usually have different instant frequencies and no standing wave pattern is created. The time-averaged intensity does not change significantly compared to the mean value (1/2 in the normalized units of Fig. 4), However, when $z \sim kL/m$, where k is an integer less than m, the two interfering waves are delayed by exactly $\Delta t \sim kT_{\mathrm{FM}}$ and therefore, have nearly identical instant frequency, causing a standing wave pattern to reappear. Therefore, the spatial hole burning is not completely mitigated, as shown in Fig. 4(a), there are still m regions in the which spatial hole burning occurs. Since $T_{\mathrm{FM}} \sim \tau_2$, in a typical THz QCL m is on the order of 25 to 30. For mid-IR lasers, this number may be even larger due to shorter gain recovery times.

Now, consider the case when the FM frequency $\nu_{\mathrm{FM}}(t)$ is no longer constant but a function of time and oscillates randomly within the bounds $\bar{\nu}_{\mathrm{FM}} \pm \Delta\nu_{\mathrm{FM}}/2$; the only restraint placed on it being $\nu_{\mathrm{FM}}(t + \tau_{\mathrm{rt}}) = \nu_{\mathrm{FM}}(t)$. The mean period $\bar{T}_{\mathrm{FM}} = \bar{\nu}_{\mathrm{FM}}^{-1}$ is commensurate with the gain recovery and the parameter $\delta_{\mathrm{FM}} = \Delta\nu_{\mathrm{FM}}/2\bar{\nu}_{\mathrm{FM}}$ describes "randomness" of the FM. This FM signal is shown in the inset of Fig. 4(b), which illustrates the spatial pattern created by its propagating in the cavity. Clearly, the standing wave pattern gets suppressed through the entire length of the cavity and the spatial hole burning is mitigated.

Before we embark on a rigorous numerical analysis on how the "randomization" affects the laser threshold and efficiency, we provide a rough semianalytical estimate of the effect of spatial hole burning. Consider the power density distribution inside the cavity $p(z,t)$, normalized to the saturation power density. The gain medium acts as an "integrator" with the characteristic time equal to the gain recovery time, i.e., it responds to the averaged power

$$\langle p(z,t)\rangle_{\tau_2} = \int_{-\infty}^{t} p(z,\tau)e^{\frac{\tau-t}{\tau_2}}\mathrm{d}\tau = \bar{p} + \delta p(z,t), \quad (26)$$

where the second term describes the spatial variations in $p(z,t)$, occurring on a time scale longer than the gain recovery time, to which the gain medium can actually react. If the uniform unsaturated gain in the medium is γ_0, it then saturates as $\gamma(z,t) = \gamma_0/[1 + p(z,t)]$. The average gain experienced by the photon is then

$$\bar{\gamma} = \frac{\langle\gamma(z,t)p(z,t)\rangle_{z,t}}{\bar{p}} = \frac{\gamma_0}{\bar{p}}\left\langle\frac{\bar{p} + \delta p(z,t)}{1 + \bar{p} + \delta p(z,t)}\right\rangle_{z,t} \approx \frac{\gamma_0}{1+\bar{p}}\left[1 - \frac{\langle\delta p^2\rangle_{z,t}}{\bar{p}(1+\bar{p})^2}\right] \approx \frac{\gamma_0}{1+\bar{p}}[1 - \bar{p}\sigma_p^2], \quad (27)$$

where the variance is defined as

$$\sigma_p^2 = \langle\delta p^2(x,t)\rangle_{t,z}/\bar{p}^2. \quad (28)$$

Furthermore, the relaxation current itself is proportional to the gain

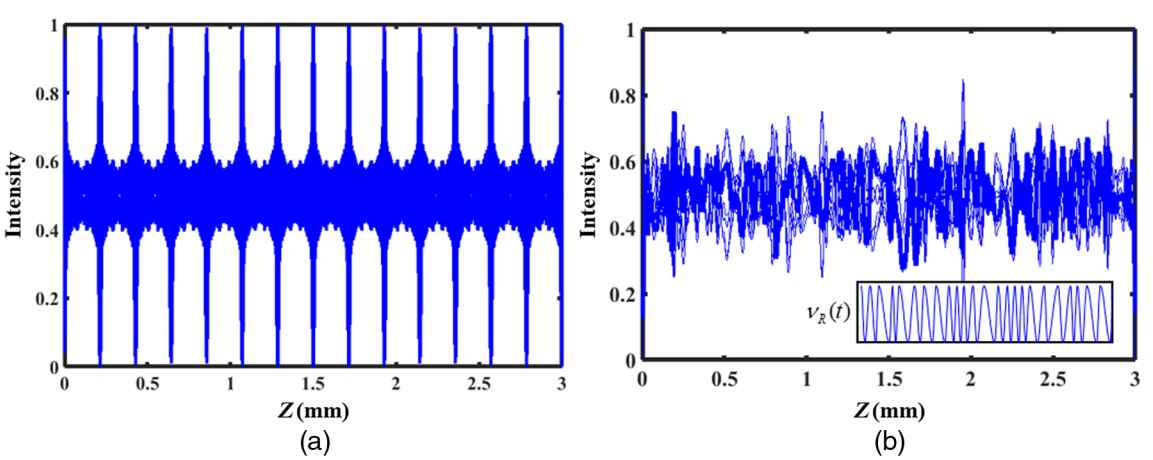

Fig. 4 (a) Intensity pattern for a deterministic FM signal in a cavity (b) intensity envelope for a stochastically FM signal. Cavity length is 3 mm with $m = 14$.

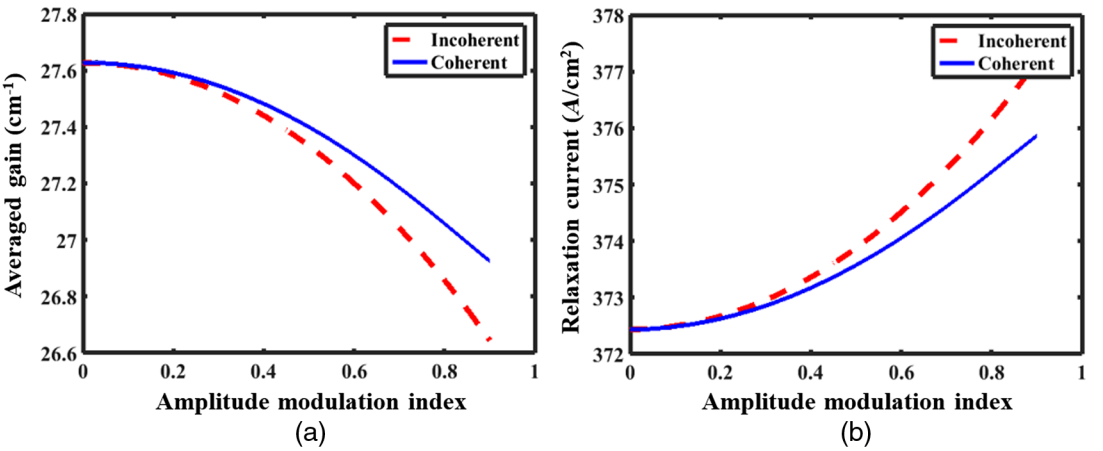

Fig. 5 The effect of amplitude modulation on (a) gain and (b) nonradiative decay.

$$\bar{J}_{\mathrm{rel}} \sim \langle \gamma(z,t) \rangle_{z,t} = \gamma_0 \left\langle \frac{1}{1+\bar{p}+\delta p(z,t)} \right\rangle_{z,t}$$
$$\approx \frac{\gamma_0}{1+\bar{p}} \left[1 + \frac{\langle \delta p^2 \rangle_{z,t}}{(1+\bar{p})^2} \right] \approx \frac{\gamma_0}{1+\bar{p}} [1 + \bar{p}^2 \sigma_p^2], \qquad (29)$$

indicating that, in accordance with expectations, the average gain and relaxation current behave in a complimentary fashion, just as shown in Figs. 3 and 5. For the single standing mode, one can estimate $\sigma_{p,0}^2 = \frac{1}{2\pi} \int_0^{2\pi} [2\sin^2(x) - 1]^2 = \frac{1}{2}$. This is the absolute worst-case scenario, and thus, we look for a variance much smaller than this value to show a marked improvement on the spatial hole burning of the FM signal over a nonmodulated signal. To illustrate how variance is affected by FM we have plotted, in Fig. 6(a), the variance of the intensity inside the cavity $\langle \delta p^2(x,t) \rangle_t / \bar{p}^2$ (averaged only in time) for both sinusoidal (deterministic) and pseudorandom FM spectra. In order to

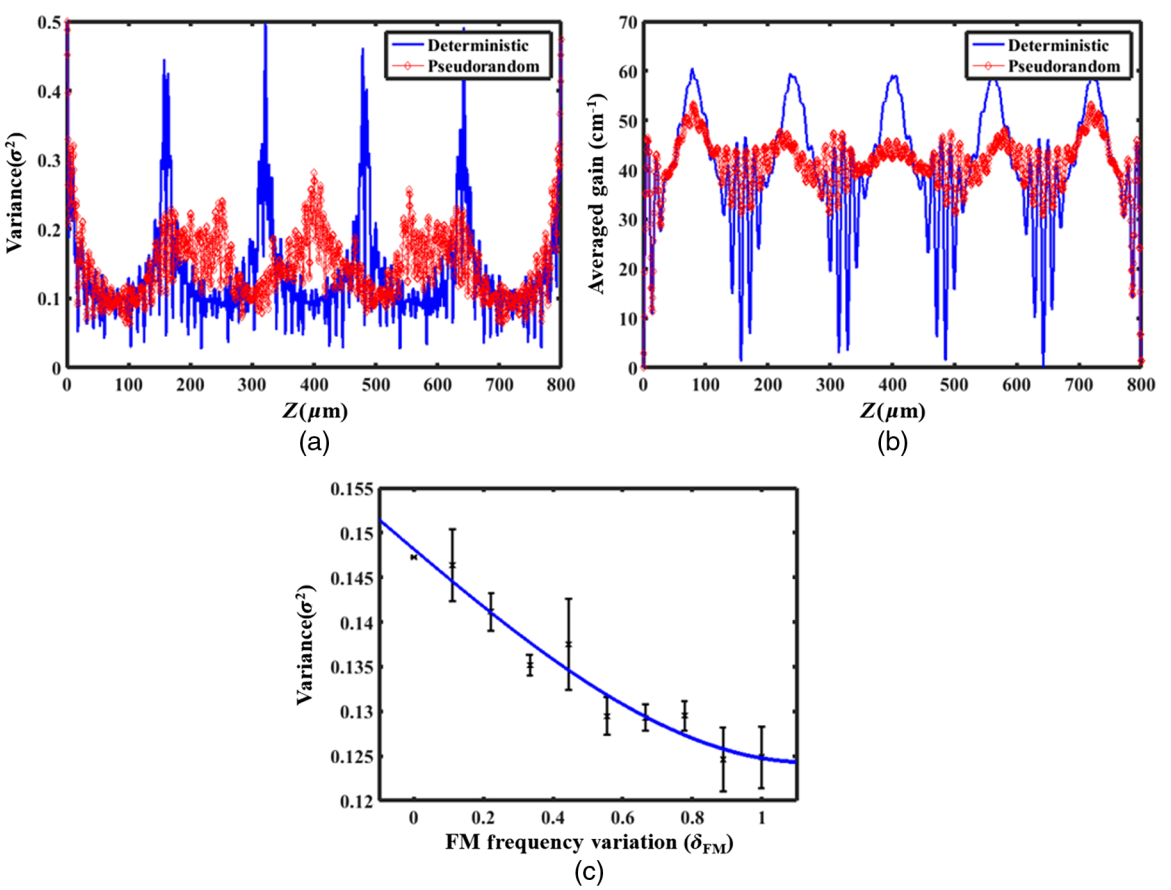

Fig. 6 (a) The spatial variance and (b) spatial gain profiles of a deterministic and pseudorandom FM spectra in an 800-μm long cavity, $m = 5$, and $\delta_{\mathrm{FM}} = 0.6$ for the pseudorandom data. (c) Averaged variance as a function of frequency variation δ_{FM}.

more clearly see the peaks in variance, we have increased the period of modulation such that $m \sim 5$. For both signals, the variance has decreased from $\sigma_{p0}^2 = 1/2$ of a nonmodulated signal. Yet for the deterministic signal, variance still peaks to a value close to half in the regions where the counter propagating signals have the same frequency. This feature is entirely suppressed in the plot for the pseudorandom signal. To show that increasing randomness of FM signal indeed suppresses spatial hole burning, we show in Fig. 6(b) spatial distribution of the gain inside the cavity. Clearly, we can see that peaks in the deterministic data show unused gain corresponding to troughs in the spatial intensity and large spatial holes that have been periodically burned. These holes are largely gone for the pseudorandom signal. The data shown in Fig. 6(c) illustrate how the variance Eq. (28) decreases with an increase of frequency variation, δ_{FM}. It is apparent that the stochasticity of our modulating signal, i.e., FM frequency variation, prevents the constructive or destructive interference of the field thus ensuring proper and uniform use of the gain with respect to spatial distribution.

7 QCL in the "Pseudorandom FM" Regime in the Presence of Spatial and Spectral Hole Burning

Now, we perform the full numerical analysis of the QCL performance for the pseudorandom FM signal. Both the effective gain $\bar{\gamma}$ and relaxation current $\bar{J}_{\mathrm{rel}}$ will be evaluated as functions of FM amplitude, A_{FM}, and the "randomness," δ_{FM}, with the average FM period $\bar{T}_{\mathrm{FM}} = 2.5$ ps. The random character of FM demands that for each value of δ_{FM}, a number of pseudorandom FM signals

$$E(z,t) = E_0 \exp\left[2\pi i \int \nu_R(t')\mathrm{d}t'\right];$$
$$\nu_R(t) = A_{\mathrm{FM}} \sin[2\pi\nu_{\mathrm{FM}}(t)t(1 + R\delta_{\mathrm{FM}})] \tag{30}$$

are generated, where the retarded time is $t' = t \mp n_{\mathrm{eff}} z/c$ with different random $\nu_R(t)$ must be generated and used for the calculations, with R being a random number from -1 to 1 and δ_{FM} scaling the randomness. These calculations can be time consuming, however, because we have already determined that within the time scale at which the FM changes the incoherent (rate equation model) is adequate our task is simplified. The initial incoherent model [Eq. (14)] is now modified to include dependencies on three dimensionalities: spectral, spatial, and temporal. Before solving the rate equation, we must first prepare an intracavity intensity that is FM and spatially dependent. This was achieved in a matter similar to Figs. 4(a) and 4(b) in which the two counterpropagating waves [Eq. (30)] are numerically superimposed upon each other, in this manner we are able to obtain a Rabi frequency that is both spatially and temporally dependent. Equation Eq. (14) is then modified as such

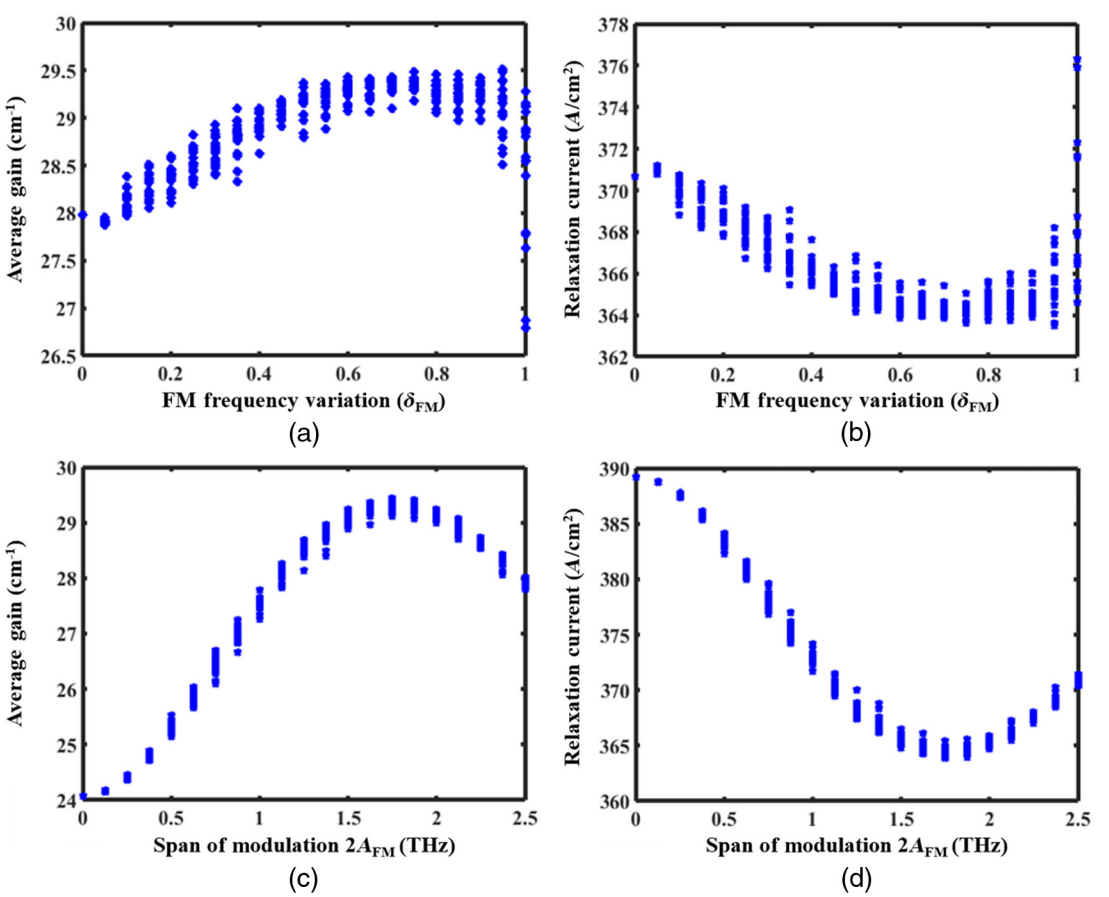

Fig. 7 (a) Average gain and (b) relaxation current versus frequency variation. (c) Average gain and (d) relaxation current versus the span of modulation, $2A_{\mathrm{FM}}$.

$$\frac{d}{d\tau}\Delta\rho^{(n)}(z,\tau) = \frac{2(\Delta\rho_o - \Delta\rho^{(n)})}{T} - \frac{\Omega'(z,\tau)^2\Delta\rho^{(n)}}{1+\Delta\omega_n'^2(z,\tau)}. \quad (31)$$

The gain and relaxation current can then be calculated similarly by averaging over both space and time as

$$\bar{\gamma} = \frac{\langle\gamma(z,\tau)\Omega'^2(z,\tau)\rangle_{z,\tau}}{\langle\Omega'^2(z,\tau)\rangle_{z,\tau}} \quad (32)$$

and

$$\bar{J}_{\text{rel}} \sim q\tau_2^{-1}N_{2\text{-D}}\langle\Delta\rho(z,\tau)\rangle_{z,\tau}. \quad (33)$$

Note that in previous sections with a constant Rabi-frequency the Ω'^2 terms in Eq. (32) cancel, however, now with a spatially dependent Rabi frequency one must be careful to include this to preserve the complimentary nature of the gain and relaxation current.

The results are shown in Fig. 7. The first two complimentary curves (a) and (b) show the effective gain and relaxation current versus the randomness parameter δ_{FM}. With many data points obtained, it is clear that the average gain reaches it maximum (and relaxation current reaches its minimum) at an optimum value of "randomness" $\delta_{\text{FM}} \approx 0.6$, in accordance with our expectations outlined above. The optimum value of FM amplitude $2A_{\text{FM}} = 1.8$ THz used in these calculations is obtained from curves (c) and (d) showing the gain and relaxation current dependence on FM amplitude. These two curves are not significantly different from the ones in Fig. 4 where the spatial hole burning was not included but the optimum value of A_{FM} is increased—apparently dealing with spatial hole burning requires stronger frequency modulation.

The cavity length used for this calculation was 800 μm, which is a few times shorter than the 5-mm cavity length in a real THz QCL. As there is now data generated for spectral, spatial, and temporal domains, a more realistic cavity length would require too high a level of computing power. In the data presented here, there are 41 spectral bins, z-based calculations are done every $\lambda/60$, and temporal calculations are performed every $\tau_{\text{rt}}/1000$, giving very large 3-D arrays. However, as one can see from Figs. 6(a) and 6(b), the difference in the spatial patterns of hole burning is already well established with a shorter cavity length and one should not expect that further enlarging the number of spatial points in our calculations will change neither the trend nor the conclusions of this paper.

Due to the random nature of our model as well as the subtle scale upon which the variables δ_{FM} and A_{FM} affect the laser, much averaging must be performed. Even so, there is a very clear trend that as spatial variance decreases with the increasingly stochastic nature of our modulating signal, so does spatial hole burning. This stochastic frequency modulation in turn reduces both spatial and spectral hole burning to a much shallower and broader regime, offering a more efficient use of the gain and lower threshold.

8 Conclusion

In conclusion, we have addressed the origin of FC formation in free-running QCLs. The QCL naturally frequency modulates its spectra in order to suppress spatial, spectral, and temporal hole burning. The frequency modulation itself mitigates spectral hole burning and produces a CW intensity, favorable to the fast saturable gain medium. The nature of the FM signal mismatches modal frequencies in space to prevent spatial and temporal hole burning. This natural mitigating behavior has been observed in various gain media and optical configurations. For example, in order to maximize coherent radiation, light sent through a ring resonator with optical gain tends to propagate only in one direction to avoid spatial hole burning. Another example is multiple pulses circulating a cavity will "choose" to collide in the saturable absorber rather than in the gain medium showing a preference for mitigating gain saturation.[31] We have thus shown here that a pseudorandom self-FM is a "natural" mode of operation as has now been proven by both time-domain (here) and frequency-domain[26] models. The time-domain model presented here is 3-D (time, frequency, and space) and has been developed and then simplified, which made modeling feasible. The results presented show that when an optical field is pseudorandomly FM (as suggested by the experimental data[4,18]), the QCL operates in the most efficient regime with a larger fraction of the pump power converted into optical radiation rather than diverted into nonradiative relaxation. Therefore, this is a completely "natural" regime of operation that can be explained by three factors: a wide inhomogeneously broadened gain favoring multimode operation; a short gain recovery time favoring fast frequency modulation (on the scaled of τ_2); spatial hole mitigation favoring a "randomized" FM signal to avoid formation of standing waves inside the cavity.

In the end, we want to stress that goal of this work was not to develop an exact model predicting the QCL performance, as we only set out to demonstrate that the observed "pseudorandom" FM does indeed have its origin in the underlying QCL physics. That being said, we have used realistic QCL parameters and obtained values of gain and laser power in an agreement with typical values obtained in the experiment. Therefore, we believe that while our model can hardly be qualified as a "design tool" for QCL development, it is nevertheless helpful to the FC community as it explains this "natural" FC formation without any external perturbations. It is worth mentioning that although we used values typical for a THz QCL, this explanation is also relevant to mid-IR lasers with some potential differences as will be further investigated in our ongoing work aimed at a better understanding of the fascinating dynamics in QCL's.

Acknowledgments

The authors acknowledge generous support provided by DARPA SCOUT program.

References

1. J. Faist et al., "Quantum cascade laser," *Science* **264**(5158), 553–556 (1994).
2. B. S. Williams, "Terahertz quantum-cascade lasers," *Nat. Photonics* **1**(9), 517–525 (2007).
3. C. Gmachl et al., "Ultra-broadband semiconductor laser," *Nature* **415**(6874), 883–887 (2002).
4. D. Burghoff et al., "Terahertz laser frequency combs," *Nat. Photonics* **8**(6), 462–467 (2014).
5. M. Rösch et al., "Octave-spanning semiconductor laser," *Nat. Photonics* **9**(1), 42–47 (2015).
6. S. Riedi et al., "Broadband external cavity tuning in the $3-4$ μm window," *Appl. Phys. Lett.* **103**(3), 031108 (2013).
7. K. Vijayraghavan et al., "Broadly tunable terahertz generation in mid-infrared quantum cascade lasers," *Nat. Commun.* **4**, 2021 (2013).
8. I. Galli et al., "Absolute frequency measurements of CO_2 transitions at 4.3 μm with a comb-referenced quantum cascade laser," *Mol. Phys.* **111**(14–15), 2041–2045 (2013).

9. T. Udem, R. Holzwarth, and T. W. Hänsch, "Optical frequency metrology," *Nature* **416**(6877), 233–237 (2002).
10. T. J. Kippenberg, R. Holzwarth, and S. Diddams, "Microresonator-based optical frequency combs," *Science* **332**(6029), 555–559 (2011).
11. T. M. Fortier, A. Bartels, and S. A. Diddams, "Octave-spanning Ti: sapphire laser with a repetition rate >1 GHz for optical frequency measurements and comparisons," *Opt. Lett.* **31**(7), 1011–1013 (2006).
12. B. R. Washburn et al., "Phase-locked, erbium-fiber-laser-based frequency comb in the near infrared," *Opt. Lett.* **29**(3), 250–252 (2004).
13. A. Schliesser, N. Picqué, and T. W. Hänsch, "Mid-infrared frequency combs," *Nat. Photonics* **6**(7), 440–449 (2012).
14. C. Y. Wang et al., "Coherent instabilities in a semiconductor laser with fast gain recovery," *Phys. Rev. A* **75**(3), 031802 (2007).
15. S. Barbieri et al., "Coherent sampling of active mode-locked terahertz quantum cascade lasers and frequency synthesis," *Nat. Photonics* **5**(5), 306–313 (2011).
16. C. Y. Wang et al., "Mode-locked pulses from mid-infrared quantum cascade lasers," *Opt. Express* **17**(15), 12929–12943 (2009).
17. D. Revin et al., "Active mode locking of quantum cascade lasers in an external ring cavity," *Nat. Commun.* **7**, 11440 (2016).
18. A. Hugi et al., "Mid-infrared frequency comb based on a quantum cascade laser," *Nature* **492**(7428), 229–233 (2012).
19. Q. Lu et al., "High power frequency comb based on mid-infrared quantum cascade laser at $\lambda \sim 9$ μm," *Appl. Phys. Lett.* **106**(5), 051105 (2015).
20. S. Bartalini et al., "Frequency-comb-assisted terahertz quantum cascade laser spectroscopy," *Phys. Rev. X* **4**(2), 021006 (2014).
21. F. Cappelli et al., "Frequency stability characterization of a quantum cascade laser frequency comb," *Laser Photonics Rev.* **10**(4), 623–630 (2016).
22. G. Villares et al., "Dual-comb spectroscopy based on quantum-cascade-laser frequency combs," *Nat. Commun.* **5**, 5192 (2014).
23. Y. Yang et al., "Terahertz multiheterodyne spectroscopy using laser frequency combs," *Optica* **3**(5), 499–502 (2016).
24. L. F. Tiemeijer et al., "Passive FM locking in InGaAsP semiconductor lasers," *IEEE J. Quantum Electron.* **25**(6), 1385–1392 (1989).
25. J. Faist et al., "Distributed feedback quantum cascade lasers," *Appl. Phys. Lett.* **70**(20), 2670–2672 (1997).
26. J. Khurgin et al., "Coherent frequency combs produced by self frequency modulation in quantum cascade lasers," *Appl. Phys. Lett.* **104**(8), 081118 (2014).
27. S. Kumar, Q. Hu, and J. L. Reno, "186 K operation of terahertz quantum-cascade lasers based on a diagonal design," *Appl. Phys. Lett.* **94**(13), 131105 (2009).
28. D. Burghoff et al., "A terahertz pulse emitter monolithically integrated with a quantum cascade laser," *Appl. Phys. Lett.* **98**(6), 061112 (2011).
29. D. Burghoff et al., "Gain measurements of scattering-assisted terahertz quantum cascade lasers," *Appl. Phys. Lett.* **100**(26), 261111 (2012).
30. D. Burghoff et al., "Evaluating the coherence and time-domain profile of quantum cascade laser frequency combs," *Opt. Express* **23**(2), 1190–1202 (2015).
31. R. Fork, B. Greene, and C. V. Shank, "Generation of optical pulses shorter than 0.1 psec by colliding pulse mode locking," *Appl. Phys. Lett.* **38**(9), 671–672 (1981).

Nathan Henry graduated from the University of New Mexico in 2012. He began working at the Night Vision and Electronic Sensors Directorate, where his research concentrated on fabrication techniques for strained-layer superlattice infrared detectors. In 2015, he decided to pursue his PhD in electrical engineering at Johns Hopkins University under the tutelage of Jacob B. Khurgin. His research is now focused on quantum cascade lasers.

David Burghoff received his PhD in electrical engineering from the Massachusetts Institute of Technology in 2014, for which he was awarded the Jin-Au Kong Doctoral Thesis Award. Since 2015, he has been a research scientist in the Research Laboratory of Electronics at MIT. His research interests lie at the intersection of quantum nanostructures, long-wavelength photonics, ultrafast optics, and computationally assisted spectroscopy.

Yang Yang received his BS degree from Zhejiang University, Hangzhou, China, in 2013. He received his MS degree in electrical engineering and computer science from MIT, Cambridge, USA, in 2015, where he is currently working toward the PhD in the areas of laser physics. Since 2013, he has been a member of Prof. Qing Hu's Group at MIT. His research interests include quantum photonics, nonlinear optics, as well as laser-based spectroscopy.

Qing Hu received his PhD in physics from Harvard University in 1987. He joined the Massachusetts Institute of Technology in 1990, where he is a distinguished professor with the Electrical Engineering and Computer Science Department. He has made significant contributions to physics and device applications over a broad spectrum, from millimeter wave, terahertz (THz), to infrared frequencies. Among those contributions, the most distinctive is his development of high-performance THz quantum cascade lasers.

Jacob B Khurgin has been a professor of electrical and computer engineering at JHU since 1988. Prior to that, he worked for seven years at Phillips NV, where he developed various display components and systems. In his almost 30 years at JHU, he has made important contributions in the fields of nonlinear optics, semiconductor optoelectronic devices, quantum-cascade lasers, optical communications, THz technology, slow light propagation, laser refrigeration of solids, plasmonics, and fundamental condensed matter physics. He is an OSA and APS fellow.